
Proceedings of the Sixth International Conference on
Railway Technology: Research, Development and Maintenance
Edited by: J. Pombo
Civil-Comp Conferences, Volume 7, Paper 15.1
Civil-Comp Press, Edinburgh, United Kingdom, 2024
ISSN: 2753-3239, doi: 10.4203/ccc.7.15.1


# Vehicle-Track-Bridge Interaction Effect in the Dynamic Response of Existing Railway Bridges

**J. C. Sánchez-Quesada,[1] E. Moliner,[1] A. Romero,[2] P. Galvín[2] and M. D. Martínez-Rodrigo[1]**

[1] **Department of Mechanical Engineering and Construction, Universitat Jaume I Castelló de la Plana, Spain**
[2] **Escuela Técnica Superior de Ingeniería, Universidad de Sevilla Spain**

## Abstract

The work presented herein is devoted to the analysis of the vertical acceleration response of high speed railway bridges composed by multiple simply-supported spans of short to medium length. In this regard, the investigation focuses on the adequacy of using highly detailed three-dimensional finite element models of the bridge for the prediction of the structural dynamic response under operational conditions. A particular bridge configuration is evaluated: pre-stressed concrete simply-supported girder bridges with high levels of obliquity. The presented bridge numerical model include: (i) a detailed discretisation of the track platform; (ii) transverse diaphragms at the span ends; and (iii) successive oblique simply-supported spans weakly coupled through the ballast track layer. To this end, digital twins of two real bridges of 15 and 25 meters span length are implemented and calibrated with experimental measurements. Different approaches for the railway vehicle are assumed to quantify the agreement between experimental and numerical predictions: (i) the simple moving load model; (ii) a multibody three-dimensional vehicle model accounting for the vehicle-bridge-interaction effect and the track irregularities. Conclusions regarding the dynamic performance and the influence of vehicle-bridge-interaction effect are finally presented.

**Keywords:** high-speed railway bridge, vertical response, three dimensional finite element model, vehicle modelling, modal superposition, track irregularities, skewness.

# 1 Introduction

The accurate assessment of train running safety on railway bridges has become an issue of major importance in the last decades. Since the opening of the first high speed (HS) railway lines worldwide, several railway bridges had experienced excessive vertical accelerations at the platform at certain speeds, leading to premature degradation of the ballast layer, the consequent loss of track stability and fatigue problems in the long term. This hazardous vibration level carries an increase in the operating costs of the line and a passenger comfort decrease [1]. Single-track bridges composed by simply-supported (SS) spans for short-to-medium length (12 - 25 m) are prone to suffer high vertical acceleration in the platform undergoing resonance due to their low mass and fundamental frequency [2]. As a result, the maximum vertical acceleration in these structures is limited to 3.5 m/s$^2$ in ballasted tracks. This dynamic threshold constitutes one of the most restrictive serviceability limit states (SLS) in the design of new structures.

Several railway bridges with pre-stressed concrete double-T girders and upper slabs for spans lengths of 10 m to 25 m were built in Spain in the 80's due to their construction facilities employing systematic procedures. Some of them are oblique in plan, in particular in the Spanish HS line Madrid-Zaragoza-Barcelona 9 skewed simply-supported bridges out of 27 were also identified. In skewed bridges, $\alpha$ is defined as the angle between the intersection of piers line and the slab cross section line. Ryájček et al. [3] present experimental and numerical results on the dynamic response of a new network arch steel railway bridge with $\alpha$ = 43° skew angle. The authors point out the sensitivity of the response to the bearings modelling, highlighting that the skewed bridges are more sensitive to boundary conditions than straight bridges. For this reason, the development of a detailed model which also includes the end transverse concrete diaphragms at the supporting sections and also the restraining effect of the ballast track between adjacent simply-supported spans is a matter of concern in this investigation. Majka and Harnett [4] analyse the effect of skewness on the response of a SS wrought-iron $\alpha$ = 26° skewed railway bridge using a 3D finite element (FE) frame model under passing three-dimensional multibody vehicle models (DBTI) for simulating the rolling stock. In this study, the computed numerical predictions considers the track irregularities. The authors conclude that the bridge skewness leads to a reduction of the vertical accelerations for speeds lower than 200 km/h. Additionally, greater accelerations were detected in the skewed case for higher speeds. Jahangiri and Zakeri [5] evaluate the effect of skewness on a 3D FE model of a concrete box girder bridge including in this case vehicle-bridge-interaction effects. In this investigation only one span length close to 25 m is analysed. The authors conclude that under passing trains, the deck vertical displacements reduce with the skew angle

but, contrarily to previous authors, not necessarily the acceleration, for which higher values are detected for speeds above 300 km/h.

In summary, given the coupling and participation of torsional and transverse-bending modes, apart from longitudinal bending mode, there are more intricacies in the dynamic behaviour of skewed bridges under railway loads than in the straight bridges. The inherently coupled three-dimensional dynamic response experienced in skewed bridges, when they are traversed by trains, motivates the use of refined three dimensional numerical models for an accurate prediction of their behaviour.

Focusing on the dynamic response of railway bridges composed by SS pre-stressed concrete multi-girder oblique decks, the aim of this work is to determine the adequacy of advanced numerical models for an accurate assessment of the SLS of vertical accelerations in these structures. This investigation covers approaches for the railway excitation ranging from the basic TLM model to more detailed multi-body vehicle models also including the vertical track unevenness. Concerning the bridge structure, highly detailed numerical models of real bridges have been implemented which include: (i) a detailed discretisation of the track platform; (ii) transverse diaphragms at the span ends; and (iii) successive oblique simply-supported spans weakly coupled through the ballast track layer. Finally, the numerical-experimental comparison of the vertical acceleration response in two real Spanish SS skewed-bridges with different span lengths is discussed.

# 2 Real bridges under study

Two existing railway bridges are studied in this investigation: the bridges over Bracea and Jabalón rivers, henceforth "Bracea bridge" and "Jabalón bridge". Both SS bridges belong to the Madrid-Sevilla High-Speed railway line and were constructed in 1991.

In Figure 1 a technical description of Bracea bridge and Jabalón bridge is shown. Bracea bridge structure presents a skew angle of $\alpha = 45^\circ$ and it is composed by two identical 15.25 m SS spans as illustrated in Figure 1(a). The deck is composed by a 0.25 m thick, 11.6 m wide, cast-in-place concrete slab resting over five 1.05 m high pre-stressed concrete I girders equispaced 2.275 m apart from the slab edges as depicted in Figure 1(c). The girders lean on two reinforced concrete abutments and one intermediate pier through laminated rubber bearings. Transverse concrete diaphragms link the deck girders at each span end. Each slab accommodates two ballast tracks with an equal eccentricity of 2.150 m, two sidewalks and handrails. The rails present a UIC60 cross section and are continuously welded. These iron path is supported by rail pads and fixed with clips on monoblock concrete sleepers with a regular spacing of 0.6 m.

As depicted in Figure 1(b), Jabalón bridge crosses the river with an oblique angle of $\alpha = 44^\circ$ using three equal spans of 24.9 m length and 11.6 m width. The outermost

spans sections are supported on two external abutments while the inner ones lean on the wall piers. As shown in Figure 1(c) both bridges are of the same typology even thought the girders height and slab thickness, with 2.050 m and 0.30 m respectively defining Jabalón bridge. For this structure the longitudinal girders are equispaced 2.517 m apart from the slab edges. Additional rubber bearings installed in the external girders restrain the transverse movement of Jabalón bridge. Finally, the ballast track layout and components are identical in both cases and its properties are listed in [6].

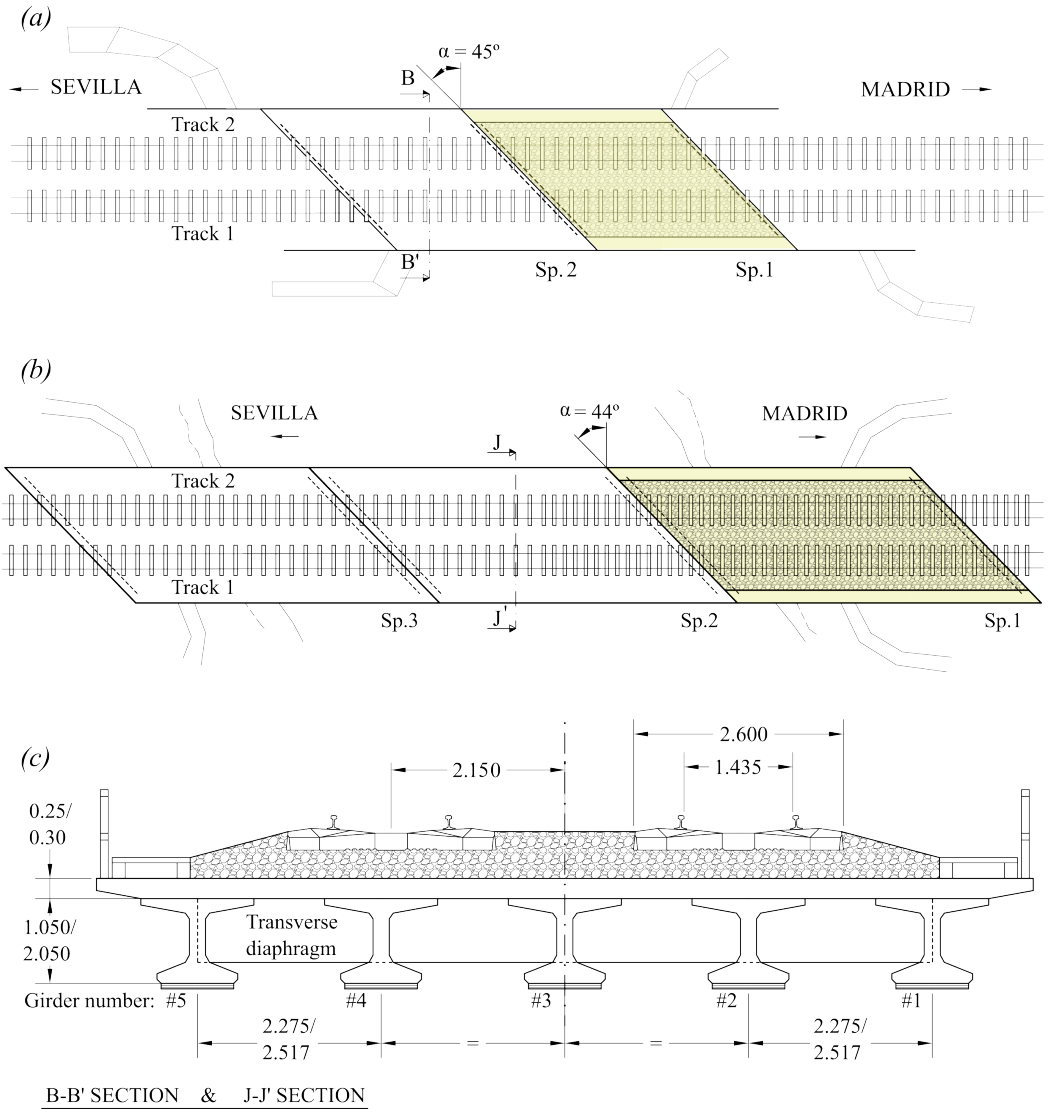


Figure 1: Technical drawings of (a) Bracea bridge top view; (b) Jabalón top view; (c) Bracea and Jabalón bridges cross-section B-B' & J-J'.

In July 2016 and in May 2019 two experimental programs were carried out by the authors to identify Arroyo Bracea and Jabalón bridges dynamic properties. In both cases, only one span of each bridge was instrumented (shaded spans in Figure 1(a-b))

with vertical accelerometers with nominal sensitivity of 10 V/g and lower frequency limit of approximately 0.1 Hz. On the bridges the vertical acceleration was recorded under operating conditions for several train passages in both directions, and also under ambient vibration. The natural frequencies and corresponding mode shapes were identified from ambient vibration by Stochastic Subspace Identification. Modal damping was obtained from the free vibrations left by the train passages, as it is considered to be more representative of the structures response under moving trains than that associated to ambient excitation.

As a result of the experimental campaigns five modes were identified in each bridge. Their mode shapes ($\Phi_i^{exp}$) are shown in Figure 2. In both cases these modes correspond to the first longitudinal-bending, first torsion, first transverse-bending, second-torsion and second-transverse bending modes of the instrumented deck in increasing frequency order. This information is used to update the digital twin models of both structures. The associated natural frequencies ($f_i^{exp}$) and free vibration damping ratios ($\zeta_{i,FV}^{exp}$) are listed in Table 1.

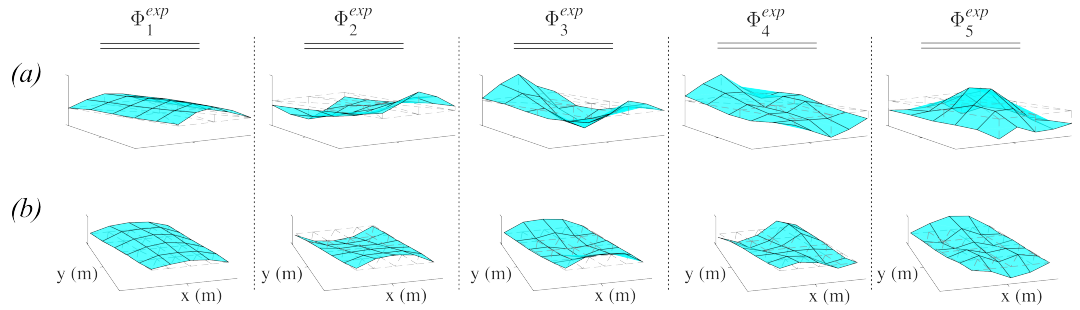


Figure 2: Experimental mode shapes identified for: (a) Bracea bridge; and (b) Jabalón bridge.

# 3 Numerical models

In this section the bridges and the vehicles models are described.

## 3.1 Detailed 3D model of the bridge structure

Two continuous 3D track-bridge FE models are implemented in ANSYS© 2020R2. These digital twins include the whole bridges, considering two or three spans for Bracea and Jabalón respectively. As for the deck, the longitudinal girders, the slab and the transverse diaphragms are meshed with isotropic Mindlin-Reissner shell FE (SHELL181) with 6 degrees of freedom (DOFs) per node. The laminated rubber bearings, located under each girder at the supports, are modelled with solid elements (SOLID185) with 3 DOFs per node, considering their real dimensions. The vertical

displacement of all the nodes at the bottom surface of the bearings is restrained, therefore ideal fixed boundary conditions are assumed and the flexibility of the piers, abutments and any interaction with the soil is neglected. Transverse bearings restraining the horizontal movement of the girders with respect to the pier cap lateral walls, only presented in Jabalón bridge, are modelled as discrete elastic springs (COMBIN14).

The ballast bed is discretised with solid FE (SOLID185). Two constitutive models are adopted over the platform: the volume of ballast along the transverse joint between adjacent spans or degraded ballast, shaded in purple in Figure 3, is considered as a transversely isotropic material, in order to take into account the possible loss of stiffness due to the relative movement caused by passing trains. This type of material permits the representation of different interlocking mechanisms of the ballast granules in the out-of-plane (vertical) and in the in-plane (horizontal) directions. For the non degraded ballast region (marked in blue in Figure 3), a linear isotropic material behaviour is considered. The sleepers are meshed into SOLID185 FE with elastic isotropic behaviour, while Timoshenko beam elements with 6 DOFs per node (BEAM188) are adopted for the rails. Finally, the rail-pads are simulated as discrete spring-dashpot elements (COMBIN14).

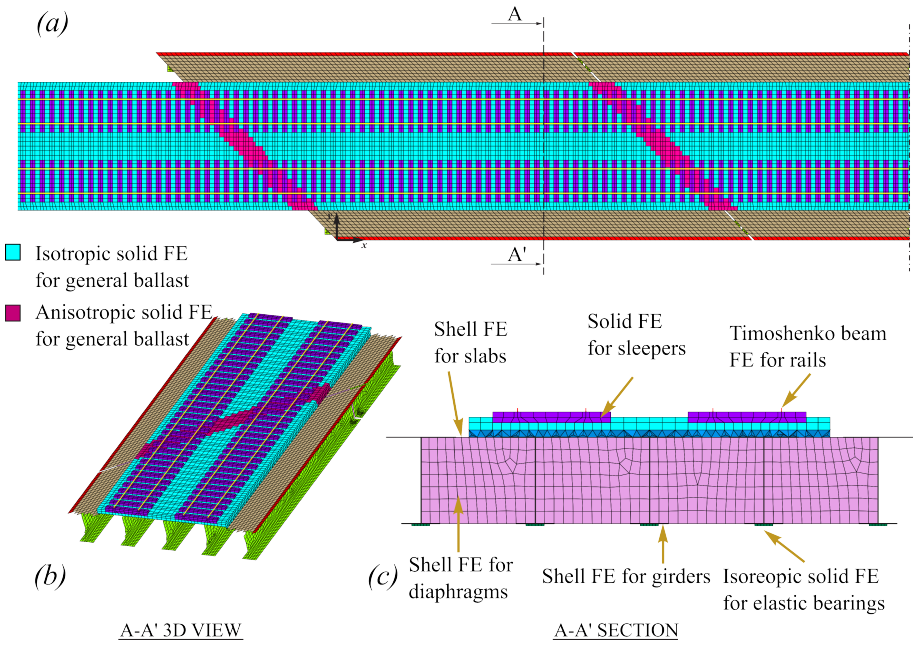


Figure 3: 3D track-bridge FE model. In the view: (a) plan view of half bridge and track extension; (b) 3D detail of deck section; and (c) AA' cross section.

A track extension of 15 m over the embankment on both sides of the bridge models is included, which is suitable according to a convergence test performed on the modal parameters. At these extensions, the ballast mesh rests on a subgrade layer, also discretised with SOLID185 isotropic elastic elements. The three translations of the nodes at the horizontal lower plane of this layer are fully restrained. The self-weight of

non-structural elements such as the handrails is included as additional lumped masses (MASS21) uniformly distributed along the two external borders. Additional density is also considered in the sidewalks areas.

A mesh convergence study was performed to guarantee an accurate prediction of the mode shapes and natural frequencies up to 30 Hz. The numerical models were subjected to a calibration procedure, similar to that described in a previous work of the authors [6], which comprises two steps. Firstly, a sensitivity analysis is conducted with the objective of choosing model parameters that have the most significant influence on the identified modes. Secondly an optimisation procedure by means of a genetic algorithm is performed, involving the use of ANSYS© 2020R2 and MATLAB© 2018b. The correspondence between experimental and numerical modal parameters is quantified through the relative difference between frequencies $e_{i,j}$ and the modal assurance criterion $\text{MAC}_{i,j}$. Table 1 presents the comparison between the experimentally identified natural frequencies and mode shapes and those predicted by the calibrated numerical models, in terms of frequency differences and MAC number for the identified modes. MAC number over 0.93 and frequency differences below 6.29 % denote enough accuracy.

| bridge | Mode | 1 | 2 | 3 | 4 | 5 |
|---|---|---|---|---|---|---|
| Bracea | $\zeta_{i,FV}^{exp}$ (%) | 3.97 | 3.24 | 2.77 | 3.61 | 4.44 |
| | $f_i^{exp}$ (Hz) | 9.25 | 10.63 | 12.75 | 17.92 | 24.57 |
| | $f_j^{num}$ (Hz) | 9.22 | 11.04 | 12.67 | 17.86 | - |
| | $e_{i,j}$ (%) | +0.3 | -3.9 | +0.6 | +0.3 | - |
| | $\text{MAC}_{i,j}$ (-) | 0.96 | 0.94 | 0.95 | 0.98 | - |
| Jabalón | $\zeta_{i,FV}^{exp}$ (%) | 3.50 | 3.30 | 2.40 | 1.10 | 1.20 |
| | $f_i^{exp}$ (Hz) | 6.30 | 7.20 | 9.30 | 24.00 | 24.50 |
| | $f_j^{num}$ (Hz) | 6.09 | 7.41 | 9.88 | - | - |
| | $e_{i,j}$ (%) | +3.4 | -2.9 | -6.3 | - | - |
| | $\text{MAC}_{i,j}$ (-) | 0.93 | 0.95 | 0.95 | - | - |

Table 1: Identified free vibration damping and experimental frequencies. Numerical frequencies, frequency differences and MAC numbers of the paired modes under 30 Hz after calibration.

## 3.2 Train model.

To evaluate the vehicle-bridge-interaction effects on the vertical acceleration levels, two different approaches are used in this study for the railway excitation modelling:

(i) the classical and well-known constant moving loads model and (ii) a multibody 3D model for the train in order to include the vehicle-bridge-interaction effect. In the refined approach, each train vehicle is modelled as a three-dimensional multi-body system, consisting of a car body, bogies and wheelsets that are regarded as rigid components. These vehicle components are connected to each other through suspension linear springs and dashpots.

During the experimental campaign performed on Arroyo Bracea I and Jabalón bridges several trains crossed the structure. Two of them were the conventional train Renfe S103 and the articulated train Renfe S100. On the one hand Renfe S103 is composed by eight equal and independent vehicles, consisting of a car body, two bogies which are independent of adjacent car's motion, and four wheelsets. With a characteristic distance of $d$ = 24.8 m, its properties can be found in [7]. On the other hand Renfe S100 is composed by ten railway vehicles: two power cars at the ends, each one directly followed by a transition car, five passenger cars and one key car. With a characteristic distance of $d$ = 18.6 m, this train has similar characteristics to Thalys HST and its physical properties and wheelsets distances are obtained from P. Galvín [8] and Y. Lee [9]. The aforementioned articulated train has a set of vehicles (transition cars, passenger cars and one key car) which are linked together through a shared bogie. Figure 4 shows the schematic representation of the trains.

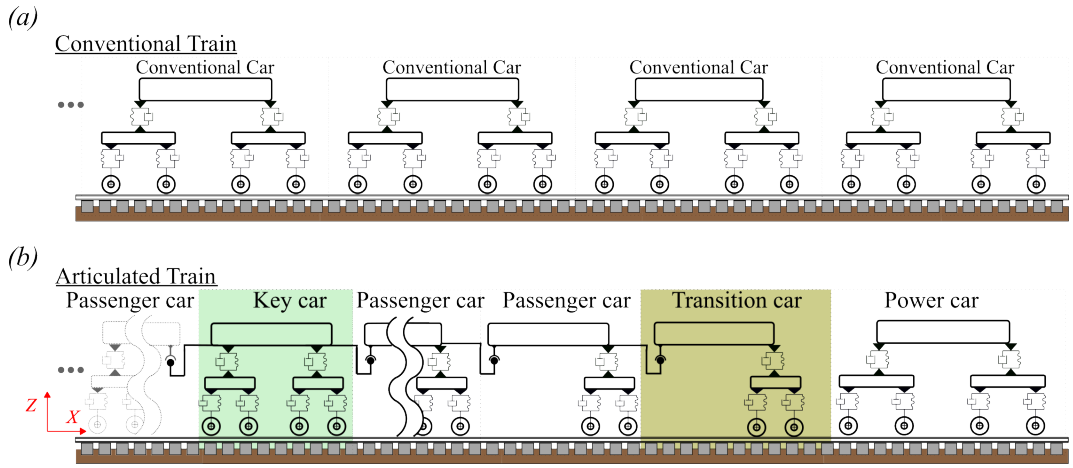


Figure 4: Train schemes: (a) Renfe S103 train; and (b) Renfe S100 train.

Frontal and side view sketches of the considered vehicle model are shown in Figure 5. Each carbody or bogie has three DOFs: vertical displacement (designated as $z^{\mathrm{C}}$ and $z^{\mathrm{B}i}$ respectively, with $i$ being the bogie number), rolling ($\theta_x^{\mathrm{C}}$ and $\theta_x^{\mathrm{B}i}$ ) and pitching ($\theta_y^{\mathrm{C}}$ and $\theta_y^{\mathrm{B}i}$ ) rotations. For each wheelset only two DOFs are considered: vertical displacement ($z^{\mathrm{W}i}$) and rolling ($\theta_x^{\mathrm{W}i}$) rotation. Therefore a 17 DOFs model is defined for a train vehicle composed by four axles (key and power cars). The coupling between the passenger car vehicles is performed through kinematic constraints, which relate the vertical displacements and pitching movements of the $(k)^{\mathrm{th}}$ car body with the vertical

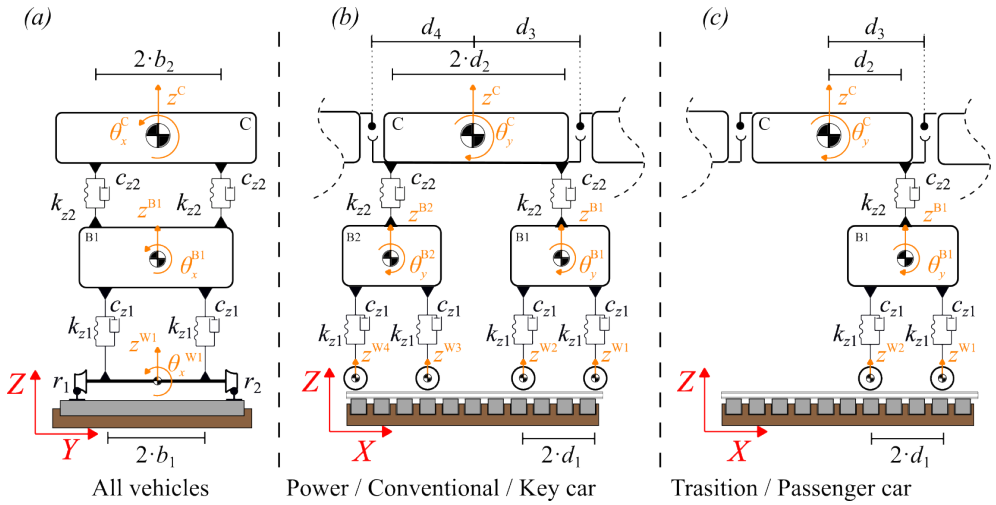


Figure 5: Vehicle model sketches: (a) Front view; (b) Lateral view of power, conventional and key cars; (c) Lateral view of transition and passenger car vehicles.

and pitching movements of the preceding one ($k$-1)$^{\text{th}}$, as is given by Equation (1), with $d_4$ and $d_3$ being the distances indicated in Figure 5.

$$z_k^{\mathrm{C}} = z_{k-1}^{\mathrm{C}} + d_{4_{(k-1)}} \cdot \theta_{y_{(k-1)}}^{\mathrm{C}} + d_{3_k} \cdot \theta_{y_k}^{\mathrm{C}} \tag{1}$$

## 3.3 Formulation of the vehicle-track-bridge interaction problem

The dynamic response of the vehicle-track-bridge system requires the solution of two coupled systems of equations. In this work, a strongly coupled approach is adopted, in which both the vehicle and the track-bridge equations are considered as a single integrated system, by enforcing compatibility of displacements at the contact points between the wheelset and the rails. A perfect contact is assumed by equating the vertical displacements of the wheelset to those of the rails after adding the track unevenness in the vertical direction (Z). For the sake of the computational effort reduction, the dynamic FE equations associated to the track-bridge subsystem are decoupled in virtue of the orthogonality of the normal modes. Therefore mode superposition is adopted to obtain the solutions for the bridge, admitting a small vehicle-to-bridge mass ratio, which is in accordance with previous works [10]. The mathematical statement of this

integrated motion system is given by Equation (2).

$$\begin{bmatrix} \mathbf{M}_v & 0 \\ 0 & \mathbf{M}_b + \mathbf{\Phi}(t)^{\mathrm{T}} \cdot \mathbf{M}_w \cdot \mathbf{\Phi}(t) \end{bmatrix} \cdot \begin{bmatrix} \ddot{\mathbf{z}}_v(t) \\ \ddot{\boldsymbol{\xi}}(t) \end{bmatrix} + \begin{bmatrix} \mathbf{C}_v & \mathbf{C}_c \cdot \mathbf{\Phi}(t) \\ \mathbf{\Phi}(t)^{\mathrm{T}} \cdot \mathbf{C}_c^{\mathrm{T}} & \mathbf{C}_b + \mathbf{\Phi}(t)^{\mathrm{T}} \cdot \mathbf{C}_w \cdot \mathbf{\Phi}(t) \end{bmatrix} \cdot \begin{bmatrix} \dot{\mathbf{z}}_v(t) \\ \dot{\boldsymbol{\xi}}(t) \end{bmatrix} + \begin{bmatrix} \mathbf{K}_v & \mathbf{K}_c \cdot \mathbf{\Phi}(t) \\ \mathbf{\Phi}(t)^{\mathrm{T}} \cdot \mathbf{K}_c^{\mathrm{T}} & \mathbf{K}_b + \mathbf{\Phi}(t)^{\mathrm{T}} \cdot \mathbf{K}_w \cdot \mathbf{\Phi}(t) \end{bmatrix} \cdot \begin{bmatrix} \mathbf{z}_v(t) \\ \boldsymbol{\xi}(t) \end{bmatrix} = \begin{bmatrix} \mathbf{P}_{cb} - \mathbf{C}_c \cdot \mathbf{T} \cdot \dot{\boldsymbol{\eta}} - \mathbf{K}_c \cdot \mathbf{T} \cdot \boldsymbol{\eta} \\ \mathbf{\Phi}(t)^{\mathrm{T}} \cdot (\mathbf{P}_w - \mathbf{M}_w \cdot \mathbf{T} \cdot \ddot{\boldsymbol{\eta}} + \mathbf{C}_w \cdot \mathbf{T} \cdot \dot{\boldsymbol{\eta}} + \mathbf{K}_w \cdot \mathbf{T} \cdot \boldsymbol{\eta}) \end{bmatrix} \tag{2}$$

$\mathbf{M}_v$, $\mathbf{C}_v$ and $\mathbf{K}_v$ stand for the sprung mass matrix of the train (bogies and car bodies), damping matrix of the car bodies (secondary suspension system) and stiffness matrix of the train (comprising car bodies and bogies), respectively. $\mathbf{M}_w$ is associated to the unsprung masses of the train (wheelsets), while $\mathbf{C}_w$ and $\mathbf{K}_w$ are the damping and stiffness matrices of the primary suspension of the train. $\mathbf{M}_b$, $\mathbf{C}_b$ and $\mathbf{K}_b$ represent the modal mass, modal damping and modal stiffness matrices of the track-bridge FE model. Due to the normalisation of the structural modes to the mass matrix, $\mathbf{M}_b$ equals the identity matrix, and $\mathbf{C}_b$ and $\mathbf{K}_b$ are diagonal matrices with $C_{b_{(i,i)}} = 2\zeta_i\omega_i$ and $K_{b_{(i,i)}} = \omega_i^2$. Finally, the system matrices $\mathbf{C}_c$ and $\mathbf{K}_c$ are the coupling terms among the DOFs of the train (car bodies and bogies) and the bridge. The term $\mathbf{\Phi}(t)$ depends on the position of the vehicle and therefore needs to be updated at each time step. This matrix relates the modal displacements of the rails with the DOFs of the wheelsets at the contact points. The vector $\mathbf{P}_{cb}$ stands for the self weight of the train suspended masses (car bodies and bogies). In the same way, the $\mathbf{P}_w$ vector contains the self weight of the wheelsets. As is stated in Equation (3), $\mathbf{T}$ is a kinematic transformation matrix which relates the DOFs of each wheelset W$i$ with the vertical displacements of the two rails of the track at the contact points, where $L_v$ refers to the track gauge.

$$\mathbf{T} = \text{diag}\,[\mathbf{T}^{\mathrm{W1}}, \mathbf{T}^{\mathrm{W2}}, \ldots, \mathbf{T}^{\mathrm{W}i}, \mathbf{T}^{\mathrm{NW}}]^{\mathrm{T}} \qquad \mathbf{T}^{\mathrm{W}i} = \begin{bmatrix} 1/2 & 1/2 \\ -1/L_v & 1/L_v \end{bmatrix} \tag{3}$$

Finally, $\boldsymbol{\eta}$ is a column vector that contains the vertical irregularity profile of the railway track at the contact points of the wheelsets, which is given by Equation (4),

$$\boldsymbol{\eta} = \text{column}\,[\boldsymbol{\eta}^{\mathrm{W1}}, \boldsymbol{\eta}^{\mathrm{W2}}, \ldots, \boldsymbol{\eta}^{\mathrm{W}i}, \boldsymbol{\eta}^{\mathrm{NW}}]^{\mathrm{T}} \qquad \boldsymbol{\eta}^{\mathrm{W}i} = [\eta_1^{\mathrm{W}i}, \eta_2^{\mathrm{W}i}]^{\mathrm{T}} \tag{4}$$

with $\eta_1^{\mathrm{W}i}$ and $\eta_2^{\mathrm{W}i}$ being the vertical irregularity profile of the rails $r1$ and $r2$ (right and left respectively) at the position of the wheelsets W$i$. The terms $\dot{\boldsymbol{\eta}}$ and $\ddot{\boldsymbol{\eta}}$ are the first and second order time derivatives of the track irregularity, which are approximated according to the chain rule. In the Equation (2), $\ddot{\mathbf{z}}_v(t)$, $\dot{\mathbf{z}}_v(t)$ and $\mathbf{z}_v(t)$ are the accelerations, velocities and displacements of the cars bodies and vehicles bogies DOFs. The $\ddot{\boldsymbol{\xi}}(t)$, $\dot{\boldsymbol{\xi}}(t)$ and $\boldsymbol{\xi}(t)$ vectors are the associated structural modal amplitudes DOFs.

The resultant equations are directly integrated in the time domain by means of Newmark beta implicit integral algorithm with $\beta$ = 1/4 and $\gamma$ = 1/2. The previous

equations are implemented in a MATLAB© 2018b code which imports the track-bridge modal parameters (natural frequencies $\omega_i$ and its respective structural mode shapes) from ANSYS© 2020R2.

# 4 Numerical-Experimental comparison

The adequacy of the implemented numerical models for the prediction of the vertical acceleration levels under the passage of the conventional and articulated trains is evaluated considering the recorded experimental measurements. The vertical acceleration recorded at different points of the decks girders in both bridges is compared with those predicted by the updated 3D FE model using different approaches for the railway excitation: (i) constant moving load model (TLM), (ii) the multibody train model described in section 3.2 including track irregularities in the vertical direction (refered to in what follows as VBI $\eta$) and (iii) the same multibody train model but neglecting track irregularities (VBI). The proposed track vertical unevenness of each rail, shown in Figure 6, is computed according to a previous work of H. Claus and W. Schiehlen [11].

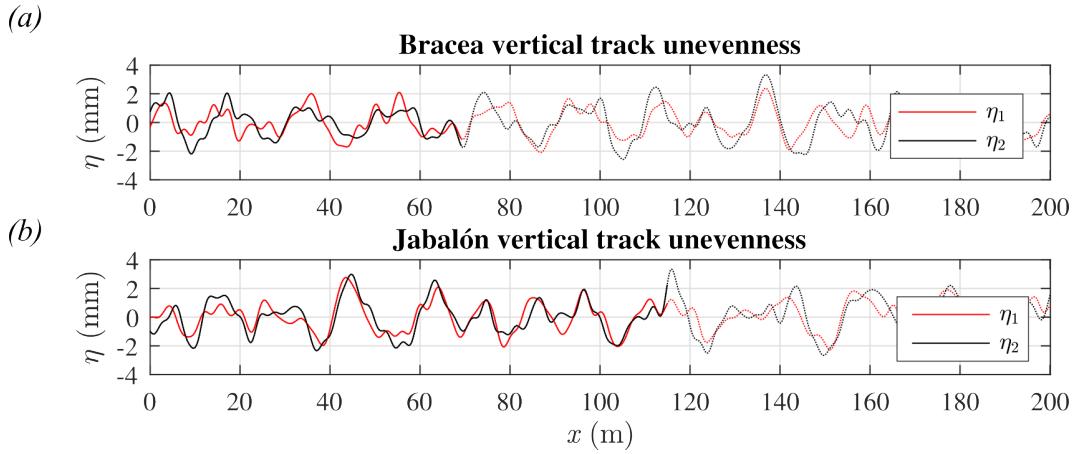


Figure 6: Track unevenness for Bracea (a) and Jabalón (b) bridges.

Mode contributions up to 30 Hz are considered in the numerical calculations as per European standards (EN 1990:2002+A1). The experimental and numerical responses are filtered applying two third-order Chebyschev filters with high-pass and low pass frequencies of 1 Hz and 30Hz respectively. Modal damping ratios identified during the experimental campaign under free vibration are assigned to the paired modes, while the recommended EC damping ratio are used for the non-paired numerical modes (EN-1991-2:2003), concretely 1.33% for Bracea bridge and 1% for Jabalón bridge numerical modes.

The conventional train Renfe S103 crossed Bracea bridge circulating over track 2 in Madrid to Seville direction at $V$ = 279 km/h and Figure 7 present the numerical-

experimental acceleration response comparison in two points underneath girders of the instrumented span. The Fast Fourier transform of the vertical acceleration, location of the measurement point and the time domain response under train passage are engaged in the same figures. The passage of Renfe S103 is interesting since the speed approaches the theoretical third order resonance velocity of the fundamental mode of the bridge, $V_{1,3} = d \cdot f_1^{exp}/3 = 24.8 \times 9.25/3 = 76.46$ m/s. In the time domain the acceleration response gradually amplifies as the train axle pass through, and also the frequency associated to the resonant mode ($f_1^{exp} = 9.25$ Hz) stand out more prominently compared to other frequency components. In the predictions presented herein, the acceleration response tend to overestimate the contribution of the resonant mode. The amplitude dependence of structural damping along with other sources of damping not included in the numerical model may contribute to decrease this discrepancies. As it is well known that the interaction between the bridge and the vehicle becomes relevant specially at resonance and under two current conditions: (i) when the frequency of the vehicle's suspended masses aligns closely with the natural frequencies of the bridge, and (ii) when the train mass is relevant when compared to the mass of the bridge. None of these situations happen in the presented train passage. The primary suspension frequency of the train model is 5.6 Hz, which is far from the fundamental frequency of the bridge (9.2 Hz). Additionally, the mass of the train does not apparently alter the natural frequencies of the structure under forced vibration.

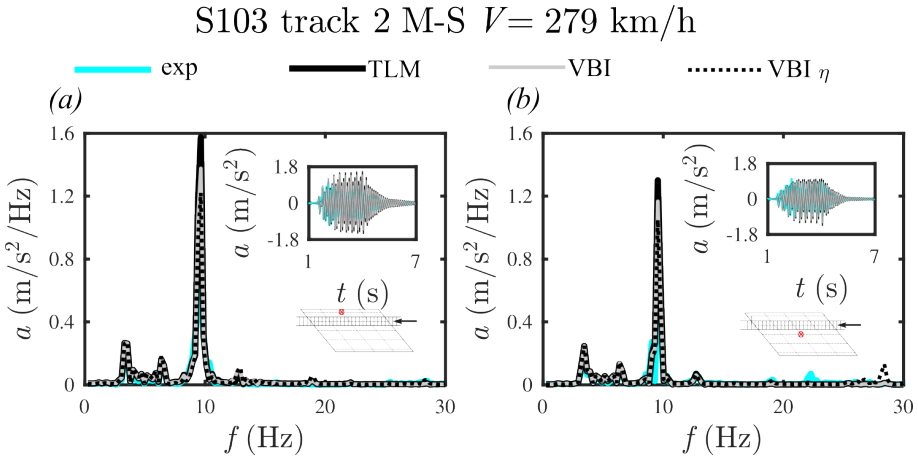


Figure 7: Acceleration induced underneath girders points of Bracea bridge when Renfe S103 traversed track 2 at speed $V$ = 279 km/h on M-S direction. Time history and frequency contents.

Finally the articulated Renfe S100 crossed Jabalón bridge over the same track and direction at $V$ = 280 km/h. Figure 8 show the numerical-experimental comparison on Jabalón bridge acceleration response in another two points underneath girders of the instrumented span. At this velocity the train passage over the structure did not induced resonance and the numerical predictions tend to underestimate the bridge response. These predictions are able to accurately predict the frequency contributions associated

to the train excitation ($f_b$ = 280/(3.6×18.6) = 4.2 Hz) and to the fundamental mode. However the correlation with the experimental measurements worsens in the range of frequencies above 15 Hz. As can be seen in Table 1 the calibrated numerical model of the Jabalón bridge predicts the natural frequencies above the third mode shape with less accuracy than the Arroyo Bracea I model, which may explain these slightly worse fit. In the case under study the degree of accuracy obtained with the TLM approach is similar than that of the VBI model for the prediction of the vertical acceleration of the deck, since the inertial effects of the vehicles are negligible.

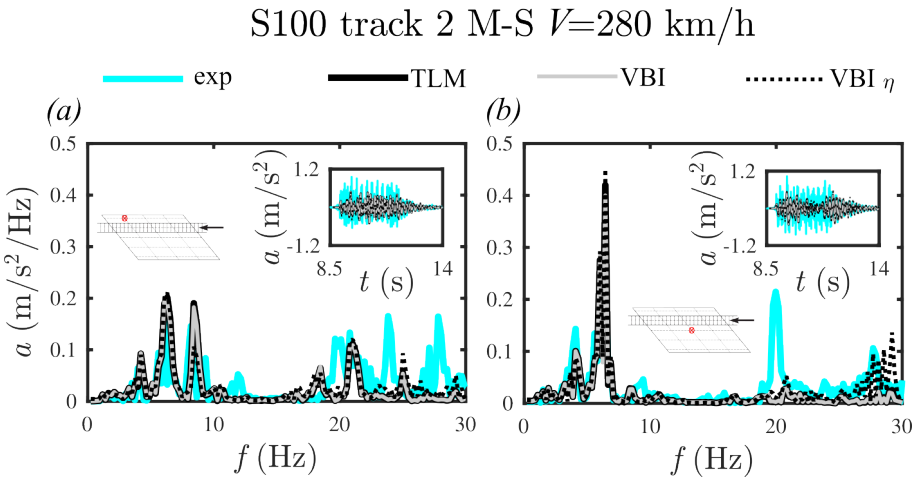


Figure 8: Acceleration induced underneath girders points of Jabalón bridge when Renfe S100 traversed track 2 at speed $V$ = 280 km/h on M-S direction. Time history and frequency contents.

# 5 Conclusions & contributions

The implementation and updating of realistic numerical models of highly-skewed multi-girder bridges is more complex than that of straight ones, due to the dependence of their dynamic properties on the boundary conditions, and to the participation of three dimensional modes such us transverse bending or torsion in the dynamic response under passing trains. Regarding the numerical-experimental comparison under non resonant conditions, the frequency content of the forced structural response exhibits the participation of several frequency contributions. These frequencies are well predicted by the numerical models and are clearly visible in the frequency range [1-11 Hz] of the deck acceleration response, which is attributed to the successful updating of the FE models with experimental data. However, the fitting between measured and predicted levels of accelerations worsen at higher frequencies, since the FE model reproduces whit less accuracy frequency contents above 11 Hz. For this reason, the correlation with the experimental measurements improves under resonant train passages. Additionally, the inertial effects of the circulating vehicles and their suspension

systems have small relevance in predicting the vertical acceleration levels on the existing bridges studied in this research. The implemented numerical models tend to overestimate the bridge resonant response, while the vibratory levels under non resonant conditions are underestimated. The non linearity of damping mechanisms along with the inherent difficulty in estimating reliable modal damping parameters from experimental measurements, may contribute to the observed differences. Since the focus of the analysis is the dynamic response of the structure, the use of a moving mass model for the train excitation, which includes the wheel masses of the vehicles travelling at the train speed in addition to the static force from each axle, emerges as a reasonable and efficient approach to improve the correlation with the experimental measurements.

## Acknowledgements

The authors would like to acknowledge the financial support provided by the Spanish Ministry of Science (research project PID2022-138674OB-C2); Andalusian Ministry of University, Research, and Innovation (PROYEXCEL 00659); Andalusian Scientific Computing Centre; and Generalitat Valenciana (AICO/2021/200).

# References

[1] T. Isibashi, "Shinkansen structures in Japan", in "Proceeding of Workshop on bridges for High-Speed railways", Porto, Portugal, 2004.

[2] L. Frýba, "Dynamic behaviour of bridges due to high speed trains", Bridges for High-Speed Railway, CRC press, 2008, ISBN 9780429207396

[3] P. Ryjáček, M. Polák, T. Plachý, J. Kašpárek, "The dynamic behavior of the extremely skew railway bridge Oskar", in "2nd International Conference on Structural Integrity-ICSI", Funchal, Madeira, Portugal, 2017.

[4] M. Majka, M. Hartnett, "Dynamic response of bridges to moving trains: A study on effects of random track irregularities and bridge skewness", Computers and Structures, 87, 1233-1252, 2009, DOI 10.1016/j.compstruc.2008.12.004

[5] M. Jahangiri, J. Zakeri1, "Dynamic Analysis of Two-lane Skewed Bridge and High-speed Train System", Periodica Polytechnica Civil Engineering, 63 (3), 695-708, 2019, DOI 10.3311/PPci.13135

[6] J.C. Sánchez-Quesada, A. Romero, P. Galvín, E. Moliner, M.D. Martínez-Rodrigo, "3D analysis of railway induced vibrations on skew girder bridges including ballast track–bridge interaction effects", Engineering Structures, 279, 115546, 2023, DOI 10.1016/j.engstruct.2022.115546

[7] K. Nguyen, J.M. Goicolea, F. Gabaldón, "Comparison of dynamic effects of high-speed traffic load on ballasted track using a simplified two-dimensional and full three-dimensional model", Proceedings of the Institution of Mechanical Engineers Part F: Journal of Rail and Rapid Transit, 228 (2), 128-142, 2014.

[8] P. Galvín, A. Romero, J. Domínguez, “Fully three-dimensional analysis of high-speed train–track–soil-structure dynamic interaction”, Journal of Sound and Vibration, 329, 5147-5163, 2010, DOI: 10.1016/j.jsv.2010.06.016

[9] Y. Lee, S. Kim, “Structural analysis of 3D high-speed train–bridge interactions for simple train load models”, Vehicle System Dynamics, 48 (2), 263-281, 2009.

[10] K. Liu, E. Reynders, G. De Roeck, G. Lombaert, “Experimental and numerical analysis of a composite bridge for high-speed trains”, Journal of Sound and Vibration, 320, 201-220, 2009, DOI 10.1016/j.jsv.2008.07.010

[11] H. Claus, W. Schiehlen, “Modelling and simulation of railway bogie structural vibration”, Vehicle system dynamics: International Journal of Vehicle Mechanics and Mobility, 29, s1, 538-552, 1998, DOI 10.1080/00423119808969585